



## Automatic Assessment of Biometric Parameters in Optic Nerve Head Area by “Zhongshan ONH Calculator (ZOC)”

Fei Li, Kai Yu, Lichun Zhang, Kai Gao, Xinjian Chen & Xiulan Zhang

To cite this article: Fei Li, Kai Yu, Lichun Zhang, Kai Gao, Xinjian Chen & Xiulan Zhang (2018): Automatic Assessment of Biometric Parameters in Optic Nerve Head Area by “Zhongshan ONH Calculator (ZOC)”, Current Eye Research, DOI: [10.1080/02713683.2018.1563703](https://doi.org/10.1080/02713683.2018.1563703)

To link to this article: <https://doi.org/10.1080/02713683.2018.1563703>



Accepted author version posted online: 22 Dec 2018.  
Published online: 07 Feb 2019.



Submit your article to this journal [↗](#)



Article views: 18



View Crossmark data [↗](#)



# Automatic Assessment of Biometric Parameters in Optic Nerve Head Area by “Zhongshan ONH Calculator (ZOC)”

Fei Li<sup>a</sup>, Kai Yu<sup>b</sup>, Lichun Zhang<sup>b</sup>, Kai Gao<sup>a</sup>, Xinjian Chen<sup>b</sup>, and Xiulan Zhang<sup>a</sup>

<sup>a</sup>Zhongshan Ophthalmic Center, the State Key Laboratory of Ophthalmology, Sun Yat-sen University, Guangzhou, China; <sup>b</sup>School of Electronics and Information Engineering, Soochow University, Suzhou, China

## ABSTRACT

**Purpose:** To test the repeatability and reproducibility of the Zhongshan ONH Calculator (ZOC) software in terms of selected optic nerve head (ONH) parameters commonly used in clinical research of glaucoma.

**Materials and methods:** Forty-two horizontal single-line scans were selected to test the repeatability and reproducibility of the ZOC software. Clinically relevant 2D parameters of the ONH area were selected to test repeatability of ZOC, including length of BMO, minimum rim thickness on both sides (RIML and RIMR), optic cup depth (OCD), and depth of the anterior surface of the LC (ALCD).

**Results:** Intraobserver test showed higher the intra-class correlation coefficient (ICC) of BMO ((0.991 vs. 0.777), RIML (0.988 vs. 0.890), RIMR (0.972 vs. 0.846), OCD (0.997 vs. 0.992), and ALCD (0.993 vs. 0.949) by single researcher using ZOC software than manual measurement. BA analysis showed acceptable agreement between automatic and manual measurements. SDs and limits of agreement (95% CI) of BMO, RIML, RIMR, OCD, and ALCD were 0.05 (−0.13, 0.07), 0.03 (−0.05, 0.05), 0.03 (−0.06, 0.07), 0.015 (−0.035, 0.024), and 0.04 (−0.07, 0.08), respectively.

**Conclusion:** This study presented the design and development of software for the automatic measurement of OCT images of ONH area with good reproducibility. In the future, with advances of OCTs and improvements to the resolution of the LC, ZOC will become a powerful tool in glaucoma research.

## ARTICLE HISTORY

Received 21 October 2018  
Revised 18 December 2018  
Accepted 21 December 2018

## KEYWORDS

Glaucoma; optic nerve head; imaging; optical coherence tomography; software

## Introduction

Glaucoma leads to irreversible blindness through direct damage to the optic nerve.<sup>1</sup> Ocular hypertension is one of the main risk factors of glaucoma, which affects blood flow in the optic nerve head (ONH) area and triggers apoptosis of ganglion cells.<sup>2</sup> In the early stage of glaucoma, thinning of the retinal nerve fiber layer (RNFL) may be detected with an optical coherence tomography (OCT) scan of the ONH area.<sup>3,4</sup> With the progression of glaucoma, the RNFL will gradually become thinner, which is a useful landmark in the diagnosis and prediction of glaucoma. In addition to the RNFL, many other morphological changes are found at the posterior segment of human eyes, such as the optic cup, lamina cribrosa (LC), rim area (RA), etc. The LC is where the optic nerve penetrates the eyeball, which also bears abnormally high intraocular pressure (IOP) in glaucoma patients. As a result, distinct thinning of the LC can also be observed in all types of glaucoma<sup>5</sup>; the optic cup refers to the small concavity in the center of the optic disk, whose depth and volume are affected by glaucoma progression.

Measurements of the above structures were mostly taken manually for years, but this was taking too long. Poor repeatability and reproducibility exist among these data because it is

hard for humans to determine accurately the correct location on OCT images. To enhance the accuracy and efficiency of the measurements of the parameters of the ONH area, the authors developed a new algorithm and software, the “Zhongshan ONH Calculator (ZOC),” which can output automatically a series of parameters after inputting a single B-scan or three-dimensional (3D) scan OCT file. The authors also evaluated the repeatability and reproducibility of such software in terms of selected ONH parameters commonly used in glaucoma research.

## Materials and methods

### Image collection

This study was approved by the ethical community of Zhongshan Ophthalmic Center and performed in accordance to the guidelines of the Declaration of Helsinki. All participants signed an informed consent form before images were taken, and the images used in this research were all taken at the ZOC.

The DRI-OCT system (Atlantis, Topcon, Japan) was used to collect ONH images, and it uses a tunable laser with a center wavelength of 1,050 nm as a light source.

**CONTACT** Xiulan Zhang ✉ zhangxl2@mail.sysu.edu.cn 📧 Director of Clinical Research Center, Director of Institution of Drug Clinical Trials, Zhongshan Ophthalmic Center, State Key Laboratory of Ophthalmology, Sun Yat-sen University, 54S. Xianlie Road, Guangzhou 510060, China; Xinjian Chen Analysis and Visualization Lab, School of Electronics and Information Engineering, Soochow University, No. 1 Shizi Street, Suzhou City 215006, China

Fei Li and Kai Yu contributed equally to this work.

Color versions of one or more of the figures in the article can be found online at [www.tandfonline.com/icey](http://www.tandfonline.com/icey).

A horizontal single-line and 3D imaging scan procedure is performed on each participant. For horizontal scans, a scanning length of 6 mm and a scanning depth of 2.6 mm were used. Resolutions on the transverse and axial directions are 11  $\mu\text{m}$  and 10  $\mu\text{m}$ , respectively. Each 3D scan was performed in a 3 mm  $\times$  3 mm area centered on the optic disk, which was composed of 256 B-scans, each consisting of 512 A-scans (totaling 131,072 axial scans/volume).

The 2D scan images were extracted directly from the machine as 1,024  $\times$  992 pixel BMP files, while the 3D scan images were taken directly as FDS files. Images from both normal eyes and glaucomatous eyes were selected, where the latter showed obvious morphological changes in the ONH area. These two kinds of images were extracted, producing 42 images in total to test the precision and reproducibility of the software. Two images were excluded because of poor image quality on LC. Accurate segmentation of different structures in ONH area and LC relies much on the quality of OCT scans. Even experienced doctors could not determine the boundary of optic cup or LC in unclear images. Therefore, in our study we only included images with a clear view of the boundary of the optic cup and anterior surface of the LC (ALCD). In the current study, three researchers (F-L, 2-year resident doctor of ophthalmology, K-G, 5-year attending ophthalmologist specialized in glaucoma and XL-Z, professor in glaucoma) independently marked the location of bilateral BMO in the OCT images manually, while two researchers (F-L and K-G) independently measured the ONH 2D parameters manually and using ZOC software. Each image was measured by the two researchers on two separate occasions with an interval of at least seven days. For 2D images, the researcher simply imported the BMP files into the software and manually identified the locations of Bruch's membrane opening (BMO) on both sides. Although there are currently automatic algorithms recognizing BMO, in glaucoma patients its accuracy of automatic recognition are relatively poor. Therefore, we decided to manually locate BMO before measurement of other ONH biometric parameters. After manual localization of BMO, the software output each parameter automatically. For 3D images, the researcher imported the FDS files, and the whole calculation process was completed by the software without any manual operations.

### Image processing

The ZOC software is integrated with a robust algorithm designed for an ONH structure analysis. A multi-scale graph search method is used to segment three layers on ONH-centered OCT images for both 2D and 3D analysis: the internal limiting membrane (ILM), the photoreceptor inner segment/outer segment (IS/OS) junction, and the lower bound of the retinal pigment epithelium (RPE) complex. For the 2D analysis, the BMO point is user-identified, and a 2D graph search method is used to detect the LC layer in the region below the BMO reference line. For the 3D analysis, a projection image is created by averaging the voxel intensities in the z-direction between the IS/OS junction and Bruch's membrane surfaces. The optic disk and neuro-retinal rim region are detected on the projection image. The 3D LC

surface is detected by applying the graph search method to the specified region below the BMO fitted plane.

### Definition of ONH parameters

Important 2D and 3D parameters of the ONH area were selected. The 2D parameters include length of BMO, optic cup depth (OCD), depth of the ALCD, minimum rim thickness on both sides, and optic cup area (OCA). Previous research has used different definitions for these parameters.<sup>5-11</sup> However, in this research, to test the reproducibility and repeatability of the ZOC, one of the above definitions was chosen.<sup>8</sup> Length of BMO is defined as the length of the line drawn between two opening points at different sides of the ONH. Such a line is used as the reference line of the BMO plane. OCD is the largest vertical distance from any point on the contour of the optic cup to the BMO plane. Minimum rim thickness is the shortest line between BMO and any point on the contour of the ILM, measured at both sides as RIML (left) and RIMR (right). ALCD is measured by following the largest vertical distance from any point on the ALCD to the BMO plane.<sup>8</sup> Optic cup area (OCA) refers to area of optic cup under BMO reference line. (Figure 1)

3D structure of ONH could be automatically extracted from OCT scans by the ZOC software as shown in Figure 2. 3D parameters include optic cup volume (OCV), RA and average depth of anterior surface of LC (AALCD). OCV is the volume of optic cup under BMO plane. And RA is the ring-like area between optic cup and disk at BMO plane. Depth of anterior surface of LC has been described above, while AALCD refers to average depth of each point on LC to BMO reference line.

### Statistical methods

Statistical analysis was performed using STATA 14.0 (StataCorp LP, College Station, TX, USA). The intra-class correlation coefficient (ICC) was calculated to evaluate the intraobserver repeatability and agreement between different researchers. To investigate the differences between automatic and manual measurements of ONH parameters in OCT images, we also performed a Bland-Altman (BA) analysis. A value of  $P < 0.05$  was considered statistically significant.

## Result

### Baseline characteristics of images

In total, 42 pictures from 42 subjects of normal (21 pictures) and glaucomatous (21 pictures) eyes were included in this study. Demographic characteristics of participants are shown in Online Resource 1.

### Interobserver and intraobserver recognition of BMO

In total, 42 pictures of normal and glaucomatous eyes were chosen to test researchers' agreement on the recognition of BMO on the nasal side. There were excellent intraobserver

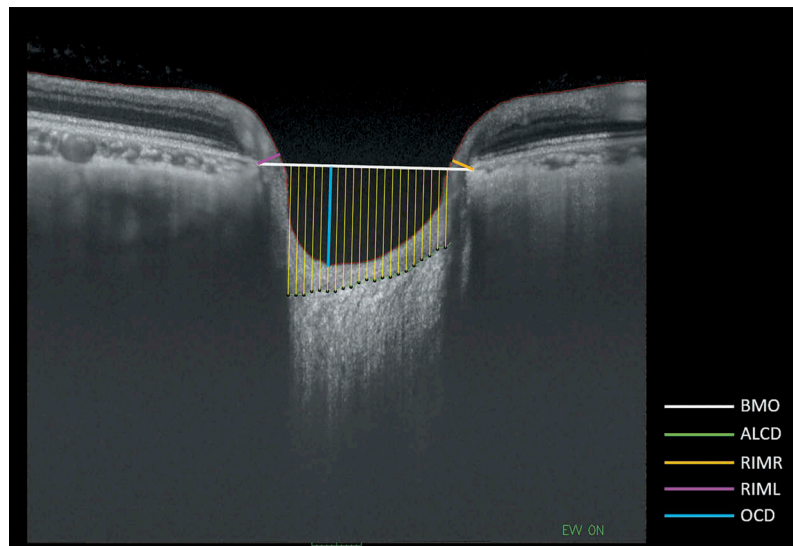


**Figure 1.** Diagram showing 2D parameters automatic measured by ZOC software, including length of Bruch's membrane opening (BMO), optic cup depth (OCD), neuroretinal rim on the left and right side (RIML and RIMR), depth of anterior surface of lamina cribrosa (ALCD), and optic cup area (OCA).

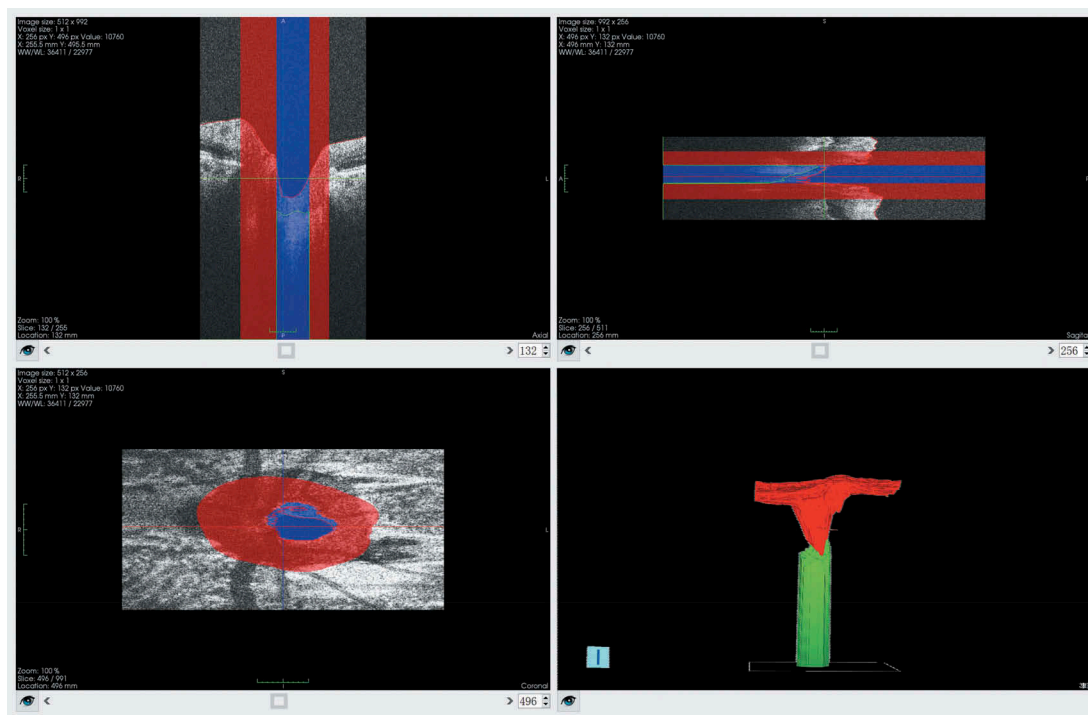


**Figure 2.** Diagram showing 3D structure of optic nerve head area extracted from OCT 3D scans by ZOC software.

and interobserver repeatability in terms of the recognition of BMO (Table 1).

### ***Intraobserver reproducibility and interobserver agreement of 2D parameters***

We compared measurement repeatability of single observer and interobserver difference between two observers using ZOC. ICC test showed no statistical significance in the repeated measurements of BMO, RIML, RIMR, OCD,

ALCD, and OCA by single researcher or between different researchers (F-L and K-G) (Table 2).

### ***Difference between manual and automatic measurements of 2D parameters***

Two researchers (F-L and K-G) also performed independently repeated manual measurements of parameters including BMO, RIML, RIMR, OCD, and ALCD. ICC test was used to compare the mean differences in repeated measurements performed by the

**Table 1.** Variation in pixel coordinates of BMO locations between repeated measurements and different observers.

BMO location	First vs. second measurement		Observer 1 vs. 2		Observer 1 vs. 3		Observer 2 vs. 3	
	ICC	<i>P</i>	ICC	<i>P</i>	ICC	<i>P</i>	ICC	<i>P</i>
x-coordiante of nasal	1.000	1.000	1.000	0.227	0.999	0.285	0.999	0.334
y-coordiante of nasal	1.000	0.690	0.999	0.265	0.999	0.304	1.000	0.321

**Table 2.** Intraobserver and interobserver agreement in the analysis of DRI-OCT images.

ONH Parameters	First observer Mean (SD)	Second observer Mean (SD)	First observer repeat ICC <sup>†</sup>	Second observer	First vs. second observer ICC <sup>†</sup>
				repeat ICC <sup>†</sup>	
BMO (mm)	1.884 (0.243)	1.878 (0.234)	0.996	0.991	0.991
RIML (mm)	0.254 (0.097)	0.246 (0.098)	0.986	0.981	0.988
RIMR (mm)	0.303 (0.158)	0.303 (0.154)	0.998	0.961	0.972
OCD (mm)	0.458 (0.159)	0.455 (0.161)	0.999	0.995	0.997
ALCD (mm)	0.541 (0.151)	0.546 (0.154)	0.995	0.992	0.993
OCA (mm <sup>2</sup> )	0.408 (0.193)	0.406 (0.194)	0.999	0.998	0.999

†Comparison using ICC test.

BMO, Bruch membrane opening; RIML, left neuroretinal rim; RIMR, right neuroretinal rim; OCD, optic cup depth; ALCD, depth of the anterior surface of the lamina cribrosa; OCA, optic cup area.

**Table 3.** Comparison of difference between interobserver difference in automatic and manual measurement.

ONH Parameters	First vs. second observer (ZOC)	First vs. second observer (manual)	ZOC vs. manual measurement (Observer 1)	ZOC vs. manual measurement (Observer 2)
	ICC <sup>†</sup>	ICC <sup>†</sup>	ICC <sup>†</sup>	ICC <sup>†</sup>
BMO (mm)	0.991	0.777	0.863	0.878
RIML (mm)	0.988	0.890	0.910	0.803
RIMR (mm)	0.972	0.846	0.912	0.803
OCD (mm)	0.997	0.992	0.985	0.980
ALCD (mm)	0.993	0.949	0.950	0.939

†Comparison using ICC test.

BMO, Bruch membrane opening; RIML, left neuroretinal rim; RIMR, right neuroretinal rim; OCD, optic cup depth; ALCD, depth of the anterior surface of the lamina cribrosa.

same researchers manually and using software. Results showed a higher interobserver ICC between repeated measurements performed by the same researchers manually or using software, which means the stability of measurements by the software is stronger than that of manual measurements (Table 3).

BA analysis showed acceptable agreement between automatic and manual measurements of ONH parameters (BMO, RIML, RIMR, OCD, and ALCD) (Figure 3). The results of SDs and limits of agreement (95% CI) of BMO, RIML, RIMR, OCD, and ALCD were 0.05 (−0.13, 0.07), 0.03 (−0.05, 0.05), 0.03 (−0.06, 0.07), 0.015 (−0.035, 0.024), and 0.04 (0.07, 0.08), respectively.

### Difference between manual and automatic measurements of 3D parameters

Manual and automatic measurements of OCV were performed in 20 eyes (10 healthy and 10 glaucomatous eyes from 20 subjects), because manual measurements of RA and AALCD could not be completed. Manual measurements of OCV were performed using the AMIRA 3D Analysis Software for Life Sciences V6.0 (FEI Company, Oregon, USA). To measure OCV in AMIRA, the optic cup under the BMO reference line was segmented on each individual slice in an OCT image. The Lasso tool was used for segmentation to avoid tissues or blood vessels near the optic cup (Figure 4).

ICC of OCV measured by ZOC and AMIRA was 0.987. BA analysis showed good agreement between automatic and manual measurements of OCV with an SD of 0.03 and limits of agreement (95% CI) of (−0.05, 0.07) (Figure 5).

## Discussion

With the invention of Fourier domain OCTs, the resolution of posterior structures has been improved vigorously. The ONH area is where the optic nerve penetrates the eyeball, and it is vulnerable to internal or external mechanic force. The morphology of the ONH area in glaucoma patients differs from that in normal subjects. Due to high IOP, ONH remodeling occurs, including deepening of the optic cup, thinning of the nerve fiber layer, etc. Observation and supervision of the morphology of the ONH area are helpful in the diagnosis and evaluation of disease conditions. Traditionally, after obtaining images of the ONH area, researchers measure relevant parameters manually, during which errors and biases arise because of humans' subjective recognition of different images.

In the present study, a novel tool was introduced for the automatic measurement of biometric parameters of the ONH area. Compared to manual measurement, the automatic estimation of parameters by computer is more accurate and takes less time. For 2D parameters, a semi-automatic measurement was utilized for, i.e., manually determining BMO points on both

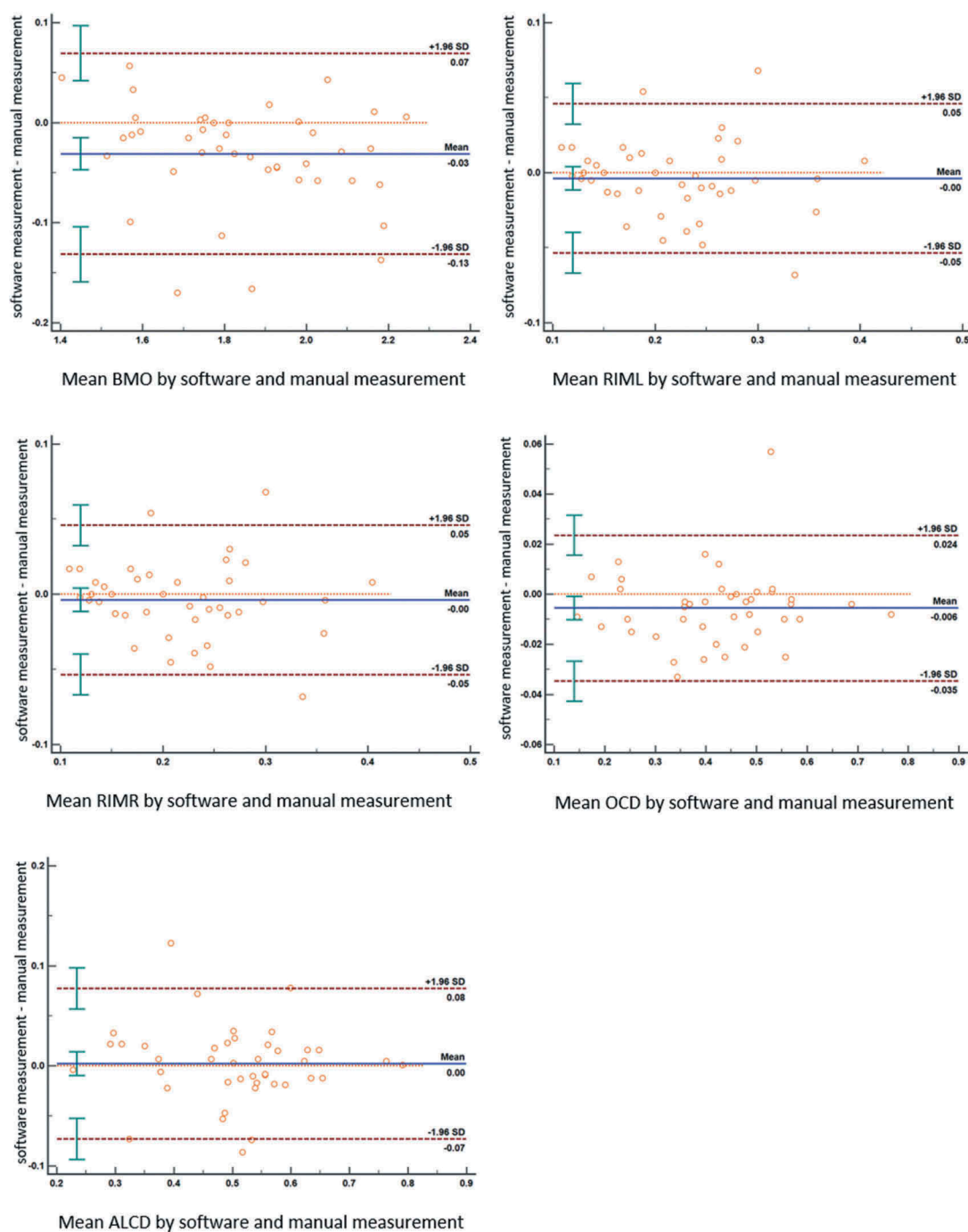


**Figure 3.** BA plot comparing measurement of 2D ONH parameters by ZOC and manually. The results of SDs and limits of agreement (95% CI) of BMO, RIML, RIMR, OCD, and ALCD were 0.05 (−0.13, 0.07), 0.03 (−0.05, 0.05), 0.03 (−0.06, 0.07), 0.015 (−0.035, 0.024), and 0.04 (−0.07, 0.08), respectively.

sides. This step could lead to possible bias in the measurement, because it cannot be guaranteed that the same pixel on the image was chosen between repeated measurements. As BMO is clearer than other ocular biomarkers, such as the scleral spur, the bias caused by BMO determination is relatively smaller, as shown in the result. After identifying BMO, the following measurement steps were completed by computers.

Six parameters on the 2D slices were chosen. In glaucoma patients, there will be detectable changes in these parameters. With the progression of glaucoma, the neuro-retinal rim will be narrowed, while the optic cup is deepened and the LC

compressed to be thinner.<sup>5,11–13</sup> Supervision of these parameters in follow-up may help determine whether there is progression of the disease or in making a diagnosis. Measurement of all the 2D parameters relies on localization of bilateral BMO. The values of BMO length and minimum rim thickness are both directly related with location of BMO, while OCD and ALCD uses the line between bilateral BMO as the reference line.<sup>8</sup> Therefore, any shift or deviation on localization of BMO will affect the accurate measurement of the above parameters. That is also the reason why we decided to manually mark BMO instead of automatic recognition by

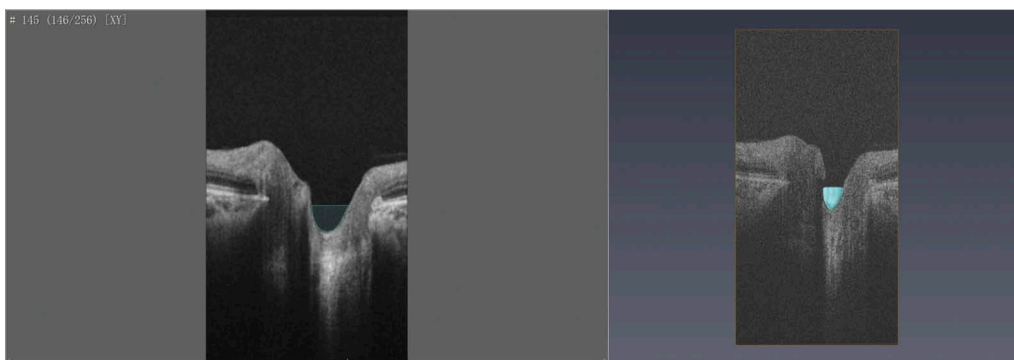


**Figure 4.** Diagram showing measurement of optic cup volume by Amira. The Lasso tool was used for segmentation to avoid tissues or blood vessels near the optic cup.

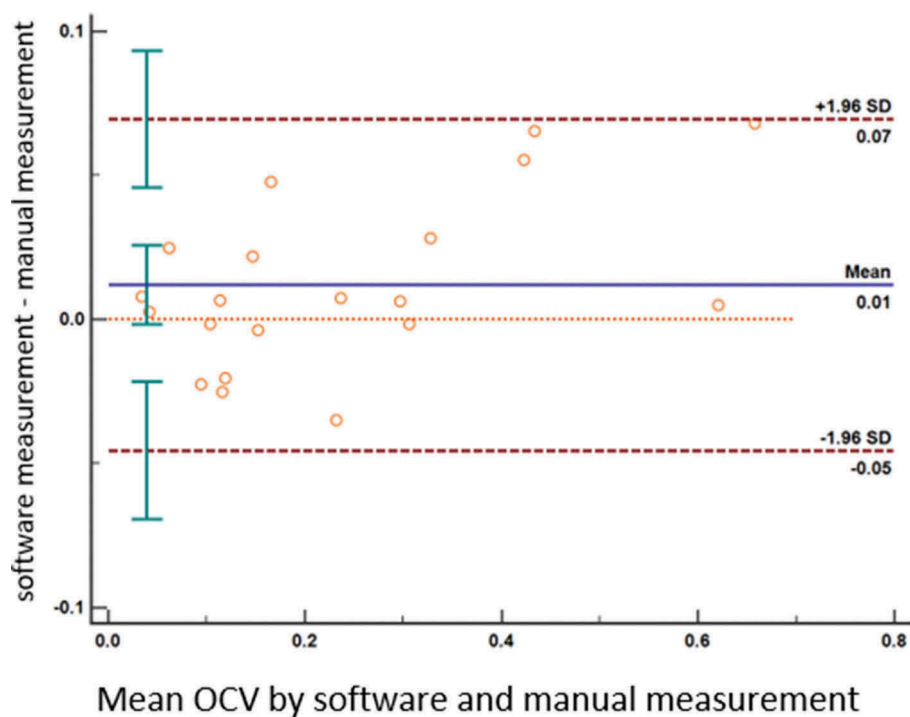


**Figure 5.** BA plot comparing OCV measurement by ZOC and Amira showing an SD of 0.03 and limits of agreement (95% CI) of  $(-0.05, 0.07)$ .

algorithm. In our study, the 3 researchers were ophthalmologists of different level. But the interobserver reproducibility was quite good. One of the reasons is that both young doctors had received training on recognition of BMO in OCT images from different subjects. Besides, we included images with clear view of optic cup and LC. The bias between different operators would become larger if more unclear images were included.

The LC is exactly where the optic nerve penetrates the eyeball, and it is the first place that glaucomatous damage occurs. Previous studies proved that LC thickness is thinner and ALCD more deepened in glaucomatous patients, and different in different types of glaucoma.<sup>7,14–16</sup> However, because of limitations in imaging technology, the inferior surface is usually not as clear as the anterior surface in OCT scans. Thus, this research did not consider LC thickness, as it is too difficult to recognize the inferior surface of the LC. For ALCD, several different measurement methods were used.<sup>8,13</sup> In this research, only the deepest point of the ALCD was measured,

because the aim was to test the reproducibility of the software. In the ZOC software, another method of measuring ALCD was also added, the same as that used in Wu's study (Figure 1).<sup>11</sup> The method in Wu's study seemed more accurate, as the entire ALCD was considered, leading to a smaller bias.

In longitudinal studies, OCT images taken at different times were analyzed together. It is difficult to ensure the same location of the ONH area is targeted when taking OCT scans. With radial scans or multiple-line scans, such problems seem solved. However, a direct analysis of 3D images always provides the most accurate and comprehensive results. Therefore, a 3D measurement of the ALCD (i.e., AALCD) was designed in the software, providing users with complete information about the ALCD. However, an accurate estimation of the AALCD depends on clear imaging of the LC, which is not easy in clinical practice. In our study, we carefully chose 20 images with clear boundary of anterior surface of LC from previous

studies. Images of 3D scans are not so clear as that in 2D scans, so we could only provide fewer qualified 3D samples. In these images, ZOC showed good agreement with manual measurement of OCV by using AMIRA. However, for the other 2 parameters, AALCD and RA, we cannot make comparison between ZOC and other methods, because we haven't seen development of measurement tools having similar functions.

Compared with the built-in software of different OCT platforms, the ZOC software has several advantages. First, when measuring 3D images, not only FDS files but also serial images of continuous slices are supported. Second, built-in software can only perform automatic measurements of 3D scans within a specific scanning area. For example, the DRI-OCT software only supports 3D scanning of the ONH area in a  $6 \times 6$ -mm region. For research aim, the  $3 \text{ mm} \times 3 \text{ mm}$  scanning mode was often used to achieve a higher resolution, and such images could not be automatically analyzed by built-in software in DRI-OCT. However, the ZOC supports 3D images of various sizes.

This study had several limitations. First, the software was tested using images from DRI-OCT, but we lacked access to all OCT brands. In the future, the authors hope to see its performance on more platforms. Second, 2D image measurements are still semi-automatic to ensure accuracy. A future aim is to design a fully automated tool.

In conclusion, this study presented the design and development of software for the automatic measurement of ONH images with good reproducibility. Improvements to the resolution of the LC and other parts in the ONH area will make the ZOC a powerful tool in glaucoma research.

## Disclosure statement

No potential conflict of interest was reported by the authors.

## Funding

This work was supported by the National Key Research and Development Project [grant number 2018YFC010302]; the Science and Technology Program of Guangzhou, China [grant number 201803010066]; and National Natural Science Foundation of China [grant number 61622114]. The funders had no role in study design or conduct, data collection and analysis, or preparation of the manuscript. The Zhongshan ONH Calculator can be accessed by contacting the corresponding author by email.

## References

- Quigley HA. Glaucoma. *Lancet*. 2011;377(9774):1367–77. doi:10.1016/S0140-6736(10)61423-7.
- Guo L, Moss SE, Alexander RA, Ali RR, Fitzke FW, Cordeiro MF. Retinal ganglion cell apoptosis in glaucoma is related to intraocular pressure and IOP-induced effects on extracellular matrix. *Invest Ophthalmol Vis Sci*. 2005;46(1):175–82. doi:10.1167/iovs.04-0832.
- Leung CK. Diagnosing glaucoma progression with optical coherence tomography. *Curr Opin Ophthalmol*. 2014;25(2):104–11. doi:10.1097/ICU.0000000000000024.
- Leung CK. Optical coherence tomography imaging for glaucoma - Today and tomorrow. *Asia Pac J Ophthalmol (Phila)*. 2016;5(1):11–16. doi:10.1097/APO.0000000000000179.
- Lee EJ, Kim TW, Kim M, Kim H. Influence of lamina cribrosa thickness and depth on the rate of progressive retinal nerve fiber layer thinning. *Ophthalmology*. 2015;122(4):721–29. doi:10.1016/j.ophtha.2014.10.007.
- Han JC, Cho SH, Sohn DY, Kee C. The characteristics of lamina cribrosa defects in myopic eyes with and without open-angle glaucoma. *Invest Ophthalmol Vis Sci*. 2016;57(2):486–94. doi:10.1167/iovs.15-17722.
- Seo JH, Kim TW, Weinreb RN. Lamina cribrosa depth in healthy eyes. *Invest Ophthalmol Vis Sci*. 2014;55(3):1241–51. doi:10.1167/iovs.13-12536.
- Jiang R, Xu L, Liu X, Chen JD, Jonas JB, Wang YX. Optic nerve head changes after short-term intraocular pressure elevation in acute primary angle-closure suspects. *Ophthalmology*. 2015;122(4):730–37. doi:10.1016/j.ophtha.2014.11.008.
- Lee EJ, Kim TW. Lamina cribrosa reversal after trabeculectomy and the rate of progressive retinal nerve fiber layer thinning. *Ophthalmology*. 2015;122(11):2234–42. doi:10.1016/j.ophtha.2015.07.020.
- Park HY, Jeon SH, Park CK. Enhanced depth imaging detects lamina cribrosa thickness differences in normal tension glaucoma and primary open-angle glaucoma. *Ophthalmology*. 2012;119(1):10–20. doi:10.1016/j.ophtha.2011.07.033.
- Wu Z, Lin C, Crowther M, Mak H, Yu M, Leung CK. Impact of rates of change of lamina cribrosa and optic nerve head surface depths on visual field progression in glaucoma. *Invest Ophthalmol Vis Sci*. 2017;58(3):1825–33. doi:10.1167/iovs.16-20509.
- Na JH, Sung KR, Lee JR, Lee KS, Baek S, Kim HK, Sohn YH. Detection of glaucomatous progression by spectral-domain optical coherence tomography. *Ophthalmology*. 2013;120(7):1388–95. doi:10.1016/j.ophtha.2012.12.014.
- Wu Z, Xu G, Weinreb RN, Yu M, Leung CK. Optic nerve head deformation in glaucoma: a prospective analysis of optic nerve head surface and lamina cribrosa surface displacement. *Ophthalmology*. 2015;122(7):1317–29. doi:10.1016/j.ophtha.2015.02.035.
- Kim YW, Kim DW, Jeung JW, Kim DM, Park KH. Peripheral lamina cribrosa depth in primary open-angle glaucoma: a swept-source optical coherence tomography study of lamina cribrosa. *Eye (Lond)*. 2015;29(10):1368–74. doi:10.1038/eye.2015.162.
- Park SC, Brumm J, Furlanetto RL, Netto C, Liu Y, Tello C, Liebmann JM, Ritch R. Lamina cribrosa depth in different stages of glaucoma. *Invest Ophthalmol Vis Sci*. 2015;56(3):2059–64. doi:10.1167/iovs.14-15540.
- Kwun Y, Han JC, Kee C. Comparison of lamina cribrosa thickness in normal tension glaucoma patients with unilateral visual field defect. *Am J Ophthalmol*. 2015;159(3):512–8 e1. doi:10.1016/j.ajo.2014.11.034.